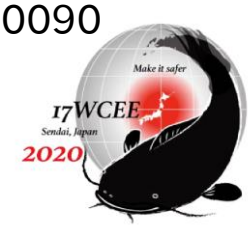

17th World Conference on Earthquake Engineering, 17WCEE
Sendai, Japan - September 13th to 18th 2020

DYNAMIC ANALYSIS OF SLENDER CONCRETE SHEAR WALLS REINFORCED WITH SUPERELASTIC SHAPE MEMORY ALLOYS

M. Maciel[(1)], W.L. Cortés-Puentes[(2)], D. Palermo[(3)]

[(1)] *Structural Engineering Intern, J.L. Richards & Associates Ltd., mmaciel@jlrichards.ca*
[(2)] *Research Associate, National Resources Canada (NRC), WilmarLeonardo.CortesPuentes@nrc-cnrc.gc.ca*
[(3)] *Vice Dean and Professor, York University, dan.palermo@lassonde.yorku.ca*

Abstract

The seismic performance of hybrid Shape Memory Alloy (SMA)-steel reinforced shear walls containing Nickel-Titanium (Ni-Ti) superelastic SMA as alternative reinforcement in the plastic hinge region was investigated with the use of nonlinear time history analysis. Two types of conventional, deformed steel-reinforced concrete shear walls were designed according to the current Canadian design standards for a prototype 10-storey office building, assuming two distinct seismic design scenarios. A moderately ductile shear wall was designed for the moderate seismic zone of eastern Canada, whereas a ductile shear wall was designed for the high seismic zone of western Canada. Equivalent hybrid SMA-steel reinforced concrete shear walls were defined from the designed cross-sections of the two conventional shear walls, in terms of geometry and reinforcement layout. Full-scale, 2-D finite element models of the walls were developed and subjected to time history analysis with selected ground motion records, including simulated and natural earthquake records, reproducing the dominant magnitude-distance scenarios of the seismic hazard of each seismic zone. Through dynamic analysis, the effects on the post-earthquake condition of the walls that are not holistically captured in static analysis, such as the effect of ratcheting, self-centering, and reduced stiffness and energy dissipation characteristics of structural elements containing SMA, are considered. The dynamic analyses demonstrated that the self-centering of SMA-reinforced concrete shear walls results in reduced permanent drifts along the height of the walls. Furthermore, comparable transient peak drifts were experienced by the SMA-reinforced walls despite the reduced stiffness and energy dissipation capacity of the walls compared to the steel-reinforced walls. In general, the use of Ni-Ti bars in the plastic hinge region illustrated the potential to optimize the seismic performance of reinforced concrete buildings, particularly in high seismic zones, controlling residual deformations and thereby reducing damage to structural elements.

Keywords: Shape Memory Alloys; dynamic analysis; reinforced concrete; seismic performance; self-centering

1. Introduction

Beyond assuring life safety, the current challenge in seismic design is to mitigate the damage that earthquakes inflict on structures, consequently reducing the loss of serviceability, recovery time, and repair costs. The seismic performance of buildings can be improved by implementing self-centering systems, using advanced materials with inherent features that are beneficial for the seismic response, such as high energy dissipation and large strain recovery. One methodology to achieving such desirable behaviour is to incorporate smart materials such as Shape Memory Alloys (SMA) into conventional structural systems. SMAs are metallic alloys with the ability to sustain large strains and to recover to a predetermined shape when heated (shape memory effect) or when loading is removed (superelastic effect). SMAs can absorb and dissipate energy by undergoing a reversible hysteretic shape change when subjected to cyclic loading. Nickel-Titanium (Ni-Ti) SMAs are of particular interest for seismic engineering applications due to characteristics such as large superelastic strain recovery, high energy dissipation, and excellent low-cycle and high-cycle fatigue properties [1].

Several researchers have successfully demonstrated the superior seismic response, with respect to self-centering, of concrete elements reinforced with SMA bars. Specifically for Reinforced Concrete (RC) shear walls, researchers have investigated, through numerical analysis, optimal locations for SMA bars in moderate and squat RC shear walls [2, 3] and in coupled shear walls [4]. The vulnerability to seismic damage of tall concrete shear walls reinforced with SMA within plastic hinge regions has been assessed with the use of fiber models and fragility curves [5]. The performance of hybrid shear walls with SMA has been evaluated and

compared to other innovative self-centering wall systems [6]. Experimental testing and numerical modelling have been used to evaluate the behaviour of slender hybrid RC walls containing SMA prior to and after repair [7]. Furthermore, experimental and numerical studies have demonstrated that hybrid SMA-steel RC shear walls can recover large inelastic displacements in spite of the presence of steel reinforcement in the web portion of the wall [8]. A numerical study on the restoring capacity of hybrid SMA-steel walls has also demonstrated the energy dissipation capabilities of SMA-reinforced concrete shear walls and the levels of axial load after which SMA does not improve the lateral response [9]. Results from these studies demonstrated excellent self-centering capacity of the hybrid SMA-steel RC walls, characterized by a stable hysteretic response with substantial energy dissipation, and acceptable serviceability performance requiring minimum repair after severe cyclic loading. However, experimental testing and modelling of hybrid SMA-steel RC shear wall systems are still limited. The complete understanding of the behaviour of this system requires further large-scale testing and numerical modelling that captures both the local and global response of SMA-reinforced walls.

In this scenario, this research intends to contribute to the advancement of the use of SMA as reinforcement in concrete structures by assessing the seismic response of full-scale, mid-rise shear walls, which are investigated using detailed Finite Element (FE), nonlinear dynamic analyses that include the behaviour of the hybrid structural system in moderate and high seismic zones. Similar lateral strength and displacement capacities, and superior restoring capacity of the SMA-reinforced walls compared to equivalent steel-reinforced walls have been demonstrated by previous nonlinear static analysis of the walls investigated herein [10]. This favourable behaviour indicates that the use of SMA as alternative reinforcement has potential to improve the seismic performance of concrete shear walls. The static analyses also demonstrated an expected lower effective stiffness of the SMA-reinforced walls, due to the lower modulus of elasticity of SMA compared to deformed steel, as well as a lower energy dissipation capacity, due to the flag-shaped hysteretic response characteristic of Ni-Ti SMA, in contrast to the wider hysteretic loops of steel-reinforced walls. The effect of the lower stiffness and reduced energy dissipation capacity on the peak lateral displacements achieved by the SMA-reinforced walls during seismic excitation, and consequent recovery capacity, will be further investigated using dynamic, time history analysis. This type of analysis provides more realistic results that properly capture the nonlinear behaviour of reinforced concrete structures.

3. Design of shear walls

A self-centering system composed by hybrid SMA-steel RC shear walls, proposed by Abdulridha and Palermo [8], was designed as the Seismic Force-Resisting System (SFRS) of a prototype 10-storey building, illustrated in Fig. 1. Four planar shear walls are provided in each principal direction of the building, which has a 3.5 m-high first storey, and nine 3.0 m-high storeys from level 2 to 10. The building configuration was adopted from a study by Sadeghian [11] with the intention to provide a prototype structure that aids the understanding of the performance of SMA-reinforced elements in full-scale structures as a pilot study. The SFRS has a simple layout and can be easily identified in the typical floor plan. The gravity-load-carrying system consists of concrete columns, which were considered not to experience inelastic response when subjected to the seismic displacements. Two types of conventional steel-reinforced concrete shear walls were designed according to the Canadian Standards Association Standard A23.3-14 Design of Concrete Structures [12] for the seismic loading defined by the 2015 National Building Code of Canada [13]. Two distinct seismic design scenarios were defined: a Ductile Steel-Reinforced Wall (Wall DSRW) was designed for the design location of Vancouver, British Columbia, while a Moderately Ductile Steel-Reinforced Wall (Wall MDSRW) was adopted for Montreal, Quebec. The walls are 6000 mm-long, with 500 mm-long boundary regions; the height is equal to 30500 mm, and the plastic hinge region is expected to extend 6050 mm from the base of the walls. Details of Walls DSRW and MDSRW, including wall thickness, are summarized in Table 1. Note that the diameter of the reinforcing bars in Table 1 correspond to 11.2 mm (10M), 16 mm (15M), and 25.4 mm (25M).

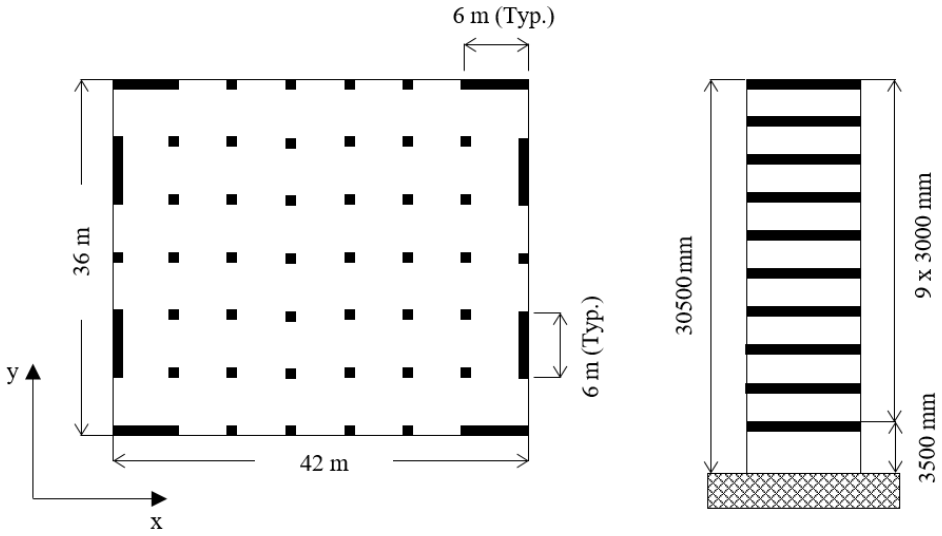

Fig. 1 – Plan view and wall elevation of the building under investigation

Table 1 – Design details of conventional steel-reinforced walls

Design details	**Wall DSRW**	**Wall MDSRW**
Wall thickness	350 mm	250 mm
Distributed reinforcement (web zone)	Two curtains of 10M @ 225 mm H	Two curtains of 10M @ 320 mm H
	Two curtains of 15M @ 230 mm V	Two curtains of 15M @ 400 mm V
Concentrated reinforcement (boundary zone)	16-25M at each end	10-25M at each end
Confinement reinforcement (boundary zone)	Three sets of 10M @ 140 mm	Two sets of 10M @ 125 mm

H and V refer to Horizontal and Vertical distributed reinforcement within the web zone of the walls

Equivalent hybrid SMA-steel RC walls, named Ductile Hybrid Wall (Wall DHW) and Moderately Ductile Hybrid Wall (Wall MDHW), were defined from the final cross-sections of Walls DSRW and MDSRW, given the lack of explicit provisions for seismic design of SMA-reinforced concrete members. The only modification was the replacement of the longitudinal steel-reinforcing bars in the plastic hinge zone within the boundaries by Ni-Ti superelastic SMA bars. The SMA bars are 25.4 mm in diameter and extend 6050 mm above the base of the walls, where the bars connect to the steel bars above the plastic hinge region through mechanical couplers modelled as stiff steel truss elements. The remaining reinforcement details were consistent with that of the steel-reinforced walls. Material properties of the reinforcing bars adopted in design and modelling of the walls are listed in Table 2. The steel strain values correspond to that employed in numerical simulations by Abdulridha and Palermo [8]. The ultimate stress and strain values of the 25.4 mm Ni-Ti SMA bars were defined assuming similar properties to that obtained by Cortés-Puentes and Palermo [14] through tension testing of 12.7 mm-diameter Ni-Ti superelastic SMA rods. The compressive strength of concrete was adopted as 30 MPa.

Table 2 – Material properties of reinforcement materials

Material property	**Steel (10M-15M)**	**Steel (25M)**	**Ni-Ti SMA**
Yield strength (f_y) - MPa	400	400	400
Ultimate strength (f_u) - MPa	600	600	1000
Modulus of elasticity (E_s) - MPa	200000	200000	38000
Strain hardening strain (ε_{sh}) - %	1.0	2.0	6.0
Ultimate strain (ε_{su}) - %	8.0	12.0	20.0

4. Numerical analysis

Nonlinear static analysis was previously used to evaluate the monotonic and hysteretic responses of Walls DSRW, DHW, MDSRW, and MDHW [10]. The numerical results were validated against experimental testing and modelling of slender, hybrid SMA-steel and conventional RC shear walls [8], [15] and against a supplementary numerical investigation of the response of the walls under varying axial load [9]. The validation of the results can be found elsewhere [10]. The static analyses were conducted with program VecTor2 [16]. The use of full-blown FE analysis was intended to permit a comprehensive understanding of the interaction of this novel material with conventional materials, evaluating potential localized effects that could not be modelled with simpler modelling tools. The same models, with minor modifications, are herein subjected to dynamic analysis.

4.1 Finite element models

The finite element models of Walls DSRW and MDHW are presented in Fig. 2. Axial load ratios ($P/A_g f'_c$) of 7% and 10% were applied as distributed storey loads at central nodes in the ductile and moderately ductile walls, respectively, which correspond to the gravity loads within the tributary area of the walls. The tributary seismic weight of each wall was converted into mass and applied to a central node at each storey. The steel reinforcement was smeared in the concrete elements throughout the models, with exception of the SMA and the steel longitudinal reinforcement in the boundaries and web zone of the walls, which were discretized with truss bar elements. The connection between SMA and steel bars was modelled as a stiff steel coupler with truss elements with diameter of 35 mm, which is greater than that of the bars.

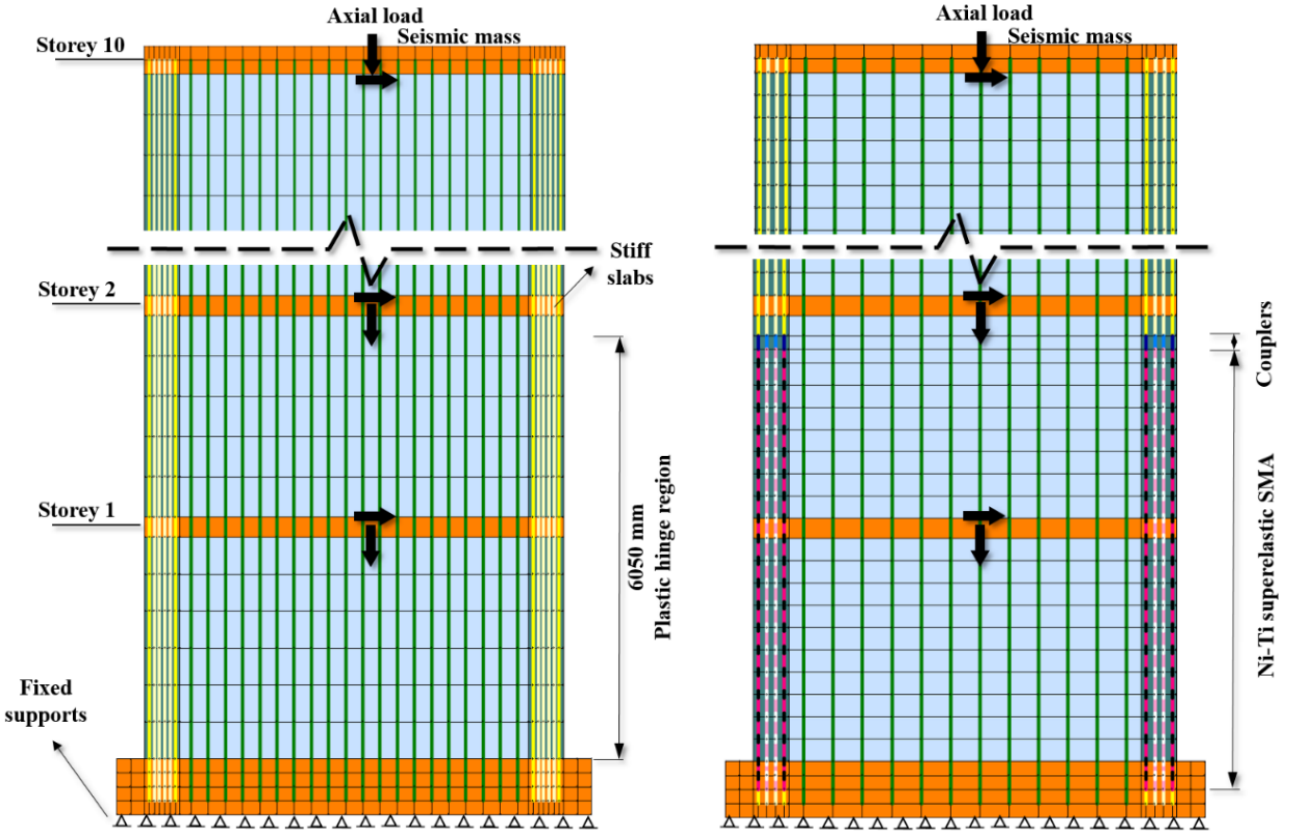

(a) (b)

Fig. 2 – Finite element models: (a) Wall DSRW and (b) Wall MDHW

The width of the slabs corresponds to the width tributary to the walls. The models also included a rigid base foundation (800 mm deep × 1500 mm wide). All deformed steel bars were considered fully bonded with

the surrounding concrete, whereas the SMA bars were modelled as embedded smooth bars interacting with the concrete rectangular elements through link elements. The Eligehausen model was used to define the stress-slip relationship of the link elements. For concrete, the compression pre-peak curve followed the Hognestad parabola, which is suitable for normal strength concrete. The descending portion of the stress-strain response (compression post-peak) was set to follow the Modified Park-Kent model. For the hysteretic response of steel, the Seckin model with Bauschinger effect was chosen. This model is composed by a linear elastic region, a subsequent yield plateau, and ultimately a curvilinear branch representing strain hardening. The hysteretic response of SMA followed the constitutive model proposed by Abdulridha et al. [17], based on a trilinear backbone envelope response. Other material models adopted in the analyses corresponded to the default material models of Program VecTor2. Detailed descriptions of these models can be found elsewhere [16].

4.2 Selection of ground motion records

To select the ground motion records employed in the dynamic analyses, the magnitude-distance (M-R) scenarios that govern each design location seismic hazard were first characterized. Thereafter, target acceleration response spectra were defined for the M-R scenarios over a period range of interest (T_R), which was computed using modal analysis to range from 0.1 s to 2.60 s for the building under study. Earthquake records were then sought to match the target response spectra of each design location using ground motion record databases. The lack of reliable historical records representative of eastern Canada motivated the use of artificial records for this seismic zone. Historical earthquake records were preferred to represent the seismic zone of western Canada, except for the megathrust events of the Cascadia subduction zone. Although the NBC 2015 [13] recommends historical earthquake records as preferred for time history analysis, the use of simulated records can ensure efficiency to the analysis, becoming appealing when natural records are not available [18].

For Vancouver, the definition of three distinct M-R scenarios is suggested given the different sources contributing to the seismicity of the region [19]. Scenarios 1 and 2 were represented by historical earthquake records from the Pacific Earthquake Engineering Research (PEER) Center database, the NGA-West2 [20], while Scenario 3 was matched with records simulating the M9 megathrust events of the Cascadia region available in the Engineering Seismology Toolbox [18] database. The final ensemble of ground motion records is presented in Table 3 in terms of characteristics of the seismic event. Fig. 3 contains the spectral acceleration of each record ($S_g(T)$), in addition to the design uniform hazard spectrum of the seismic hazard with a 2% probability of exceedance in 50 years ($S_t(T)$) defined by the NBC 2015 [13] for Vancouver, BC.

Table 3 – Characteristics of the ground motion records selected for the analysis in Vancouver

Scenario (T_R)	Record*	Record name	Distance (km)	5-95% Duration	PGA (g)	Mean $S_t(T)/S_g(T)$
1 (0.1-0.8 s)	150	Coyote Lake, 1979	3.11	3.5	0.42	1.21
	250	Mammoth Lakes, 1980	16.00	7.1	0.95	0.78
	265	Victoria, Mexico, 1980	14.37	8.2	0.65	1.23
	313	Corinth, Greece, 1981	10.27	15.4	0.24	1.28
2 (0.3-1.5 s)	14	Kern County, 1952	82.19	33.6	0.09	2.52
	359	Coalinga, 1983	26.38	10.9	0.18	1.48
	472	Morgan Hill, 1984	31.88	21.8	0.08	4.84
	496	Nahanni, Canada, 1985	4.93	4.5	0.52	1.41
3 (1.0-2.6 s)	14	M9 Cascadia 14	112.40	-	0.14	1.62
	15	M9 Cascadia 15	112.40	-	0.17	1.78
	23	M9 Cascadia 23	156.70	-	0.08	2.06

**record number as listed in the source database [20]*

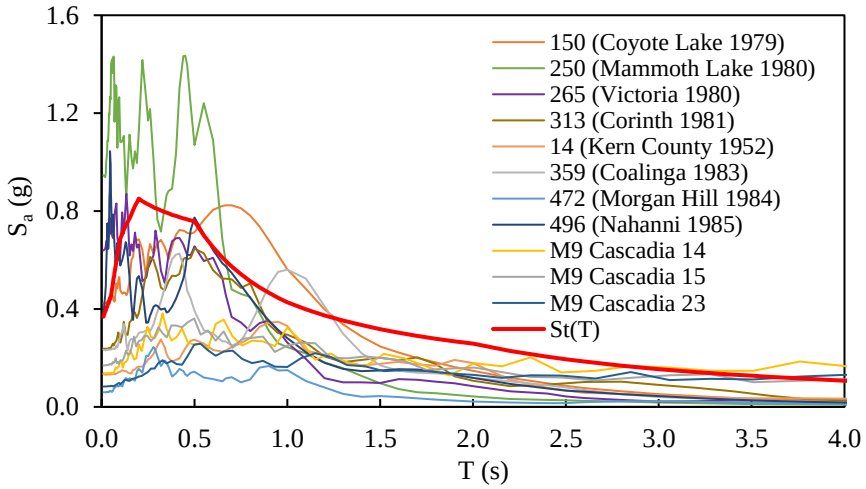

Fig. 3 – Spectral acceleration of unscaled ground motion records selected for the analysis in Vancouver

For Montreal, two dominant M-R scenarios were defined by Atkinson [18]: (1) M6 earthquakes at shorter distances influencing the shorter periods of the spectrum, and (2) M7 earthquakes at longer distances affecting the longer periods. Table 4 lists the characteristics of the eleven ground motion records chosen to represent Scenario 1 and Scenario 2 from the Engineering Seismology Toolbox [18] database of simulated ground motion records. The unscaled spectral accelerations of each selected record are illustrated in Fig. 4.

Table 4 – Characteristics of the ground motion records selected for the analysis in Montreal

Scenario (T_R)	Record*	Magnitude	Distance (km)	Duration (s)	PGA (g)	Mean $S_t(T)/S_g(T)$
1 (0.13-1.0 s)	5	6	21.5	5.0	0.28	1.34
	7		12.8	3.0	0.52	0.59
	9		12.8	3.0	0.41	0.82
	19		26.3	6.0	0.17	1.81
	30		14.3	4.0	0.50	0.82
2 (1.0-2.6 s)	6	7	50.3	18.0	0.12	1.69
	15		50.3	18.0	0.13	1.84
	18		20.6	15.0	0.49	0.78
	20		51.9	19.0	0.12	1.60
	34		25.2	16.0	0.39	1.20
	36		25.2	15.0	0.47	0.96

**record number as listed in the source database [18]*

The acceleration spectra from Fig. 3 and Fig. 4 were thereafter scaled in two stages. The first scaling factor applied was the mean of the ratio $S_t(T)/S_g(T)$, as suggested by Atkinson [18], which is presented in the last column of Table 3 and Table 4 for each record. The initial scaling process had the purpose of satisfying the NBC 2015 requirement that the selected response spectra on average equal or exceed $S_t(T)$ over the defined period range. A second single scaling factor per scenario was applied to all records in order to match the corresponding target spectra over the scenario-specific period range T_R, ensuring no point falls below 10% of $S_t(T)$.

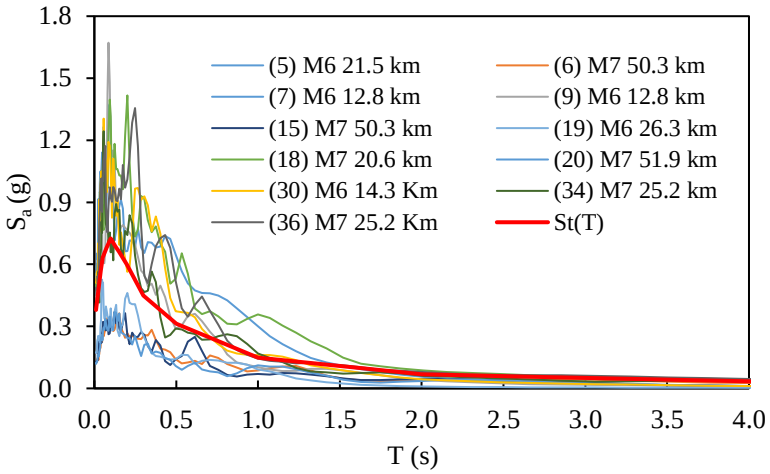

Fig. 4 – Spectral acceleration of unscaled ground motion records selected for the analysis in Montreal

5. Numerical results and discussion

Each of the four walls under study was subjected to the eleven ground motion records representative of its respective design location, resulting in a total of 44 time history analyses. The individual responses of the walls were thereafter used to compute a mean response, as suggested by the NBC 2015 [13] to deal with the great variability existing among earthquake records. The analyses were carried out for a duration that allowed the complete decay of the response of the walls in free vibration after the base excitation had ceased, permitting a more reliable calculation of the final residual deformations.

The response of the walls is evaluated in terms of lateral displacements, monitored at each storey level. Peak displacements were determined as the maximum displacement experienced at each storey during the entire analysis, while permanent displacements were recorded at the end of the analysis. Lateral drifts were thereafter calculated as the ratio of displacement to height, as roof drifts (displacement at wall top divided by wall height) and interstorey drifts (storey relative displacement divided by storey height). To evaluate the response beyond the elastic limit, peak displacements were compared to the yield displacement of the walls, Δ_y, previously determined from reverse cyclic analysis [10]. Note that yielding in SMA bars does not imply permanent inelastic deformations. Therefore, Δ_y of the SMA-reinforced walls refers to the point in the response equivalent to the yield point of the steel-reinforced walls.

5.1 Fundamental period of vibration

During the design phase, the fundamental period of the shear walls was constrained by the upper limit allowed by the NBC 2015 for determining the base shear force in shear wall buildings. The limit corresponds to two times the period calculated using the code prescribed empirical equations that are based on the wall height, and was equal to 1.3 s. Thereafter, the modal periods of vibration of the individual walls were investigated through eigenvalue analysis using VecTor2 [16], considering cracked sections by applying a factor to reduce the stiffness. The analysis resulted in the following fundamental periods of vibration: 1.73 s (Wall DSRW), 1.86 s (Wall DHW), 1.81 s (Wall MDSRW), and 1.88s (Wall MDHW). Thus, the replacement of steel bars with SMA bars in the boundaries of the walls, within the plastic hinge region, slightly increased the fundamental period of the walls by an average of 5%. The longer periods associated with the SMA-reinforced walls were expected given the lower modulus of elasticity of Ni-Ti SMA compared to that of conventional steel, as expressed in Table 2. The former results in more flexible shear wall. This reduction in stiffness, however, does not infer an inferior seismic response, as longer periods result in reduced design shear forces arising from the design uniform hazard spectrum. However, the fundamental period of the SMA-wall system was bounded by code limits, which were developed based on the response of conventional reinforced concrete shear wall systems. At the end, the design base shear employed for the SMA-reinforced walls was related to a period 31% shorter, on average, than that found using eigenvalue analysis.

5.2 Average lateral response

Fig. 5 (a) and Fig. 5 (b) illustrate the mean responses of the ductile and the moderately ductile walls, respectively, in terms of peak lateral displacements and permanent lateral displacements. The corresponding lateral drifts are presented on the secondary horizontal axis. In addition, the yield displacement of each wall is plotted for reference. In Fig. 5 (a), both ductile walls experienced similar peak lateral response, with peak roof drift in Wall DSRW corresponding to 1.5%, while Wall DHW experienced roof drift of 1.6%. Wall DSRW was able to recover 91% of the peak roof drift, while recovery in Wall DHW was equal to 99%. Wall DHW experienced peak roof drifts that were only 10% larger than Wall DSRW. In terms of interstorey drifts, the maximum interstorey drift occurred at the roof for both walls. From that, Wall DSRW recovered 93%, sustaining 0.1% permanent interstorey drift. Permanent interstorey drift in Wall DHW was 0.02%, representing 99% recovery of interstorey drifts. The results demonstrate that both walls were effective in controlling permanent drifts. Note that the earthquake records did not subject the walls to sufficiently large drifts to illustrate the difference in self-centering capacity of the two walls.

Both moderately ductile walls achieved virtually the same level of response in terms of peak drifts (Fig. 5 (b)). Wall MDHW experienced a roof drift equal to 0.49%, while Wall MDHW experienced 0.48% drift. The larger peak interstorey drifts predicted among the storey levels were equal to 0.07% and 0.1% in Walls MDHW and MDSRW, respectively. Regarding permanent drifts, there was negligible improvement in the permanent roof drift exhibited by Wall MDHW compared to that exhibited by Wall MDSRW. The recovery of Wall MDHW was 1% greater than that of Wall MDSRW. Permanent drifts were very small in both walls as a result of negligible interstorey drifts.

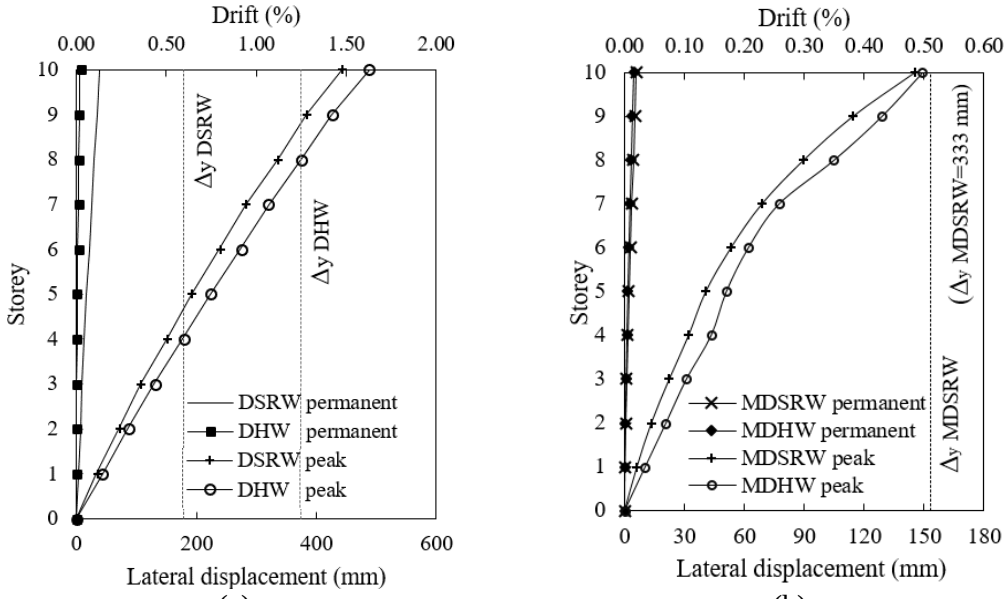

Fig. 5 – Mean lateral response: (a) ductile walls and (b) moderately ductile walls

For Vancouver, the seismic demand induced by most of the earthquake records from Scenarios 1 and 2 was sufficient to trigger yielding in Wall DSRW, but did not exceed Δ_y in Wall DHW, preventing the accumulation of inelastic deformation and resulting in recentering of the wall. At the end of the analyses from Scenarios 1 and 2, Wall DHW exhibited negligible permanent deformation. Conversely, the ground motion records from Scenario 3 exceeded the ultimate displacement, Δ_u, of the ductile walls, leading to failure. Thus, Δ_u was adopted as the peak displacement for each wall. Note that the average peak displacements in Fig. 5 (a) include Δ_u adopted for Scenario 3, which resulted in an average displacement greater than Δ_y in Wall DHW. The permanent displacements could not be evaluated due to failure and were excluded from the average response. Failure in Wall DSRW occurred due to fracture of the longitudinal reinforcement in the boundary

zone at the base of the wall, along with several adjacent bars in the web zone. In Wall DHW, failure occurred with fracture of the longitudinal steel bars in the web zone, while the SMA bars remained within the superelastic range (below 6% strain) during the entire analysis. Fracturing of the bars occurred when stresses exceeded f_u of steel. The fundamental period of the walls is encompassed by the period range of influence from Scenario 3, explaining the greater influence of this scenario in the response of the ductile walls.

For the building in Montreal, the ground motion records representative of the moderate seismic zone of Eastern Canada did not induce any notable inelastic demands in Walls MDSRW and MDHW. The response of the moderately ductile walls was more strongly influenced by records from Scenario 2 compared to Scenario 1, as the main period range affected by Scenario 2 corresponds to 1.0-2.6 s. Few of the eleven records induced displacements that were equal to or slightly above the yield displacement of the walls, resulting in an average peak displacement smaller than Δ_y. The permanent damage exhibited by the walls was limited. The superelastic capacity of the SMA reinforcement was not mobilized; in the elastic range, the beneficial effects of the superelastic SMA in Wall MDHW are not exploited. The results from dynamic analysis indicate that Eastern Canada might not be the best scenario for the implementation of self-centering, SMA-reinforced concrete shear walls, provided the level of seismic demand associated with this moderate seismic zone.

5.3 Lateral response to amplified records

It has been observed that the advantages of using SMA as alternative reinforcement in concrete are more evident when structural elements are subjected to higher seismic demands [21]. In the analyses representative of Western Canada, only a minor portion of the inelastic capacity of the walls was achieved when subjected to records from Scenarios 1 and 2, as displacements slightly exceeded Δ_y of the walls. Conversely, it was not possible to evaluate the deformed shape of the walls at the end of the analyses employing the records from Scenario 3 due to failure of the walls. For these reasons, an earthquake record from Scenario 1 was chosen and employed in the analysis with magnified acceleration time histories. The objective was to investigate the behaviour of the ductile walls when the seismic demand approaches the lateral resistance, and the demands on ductility increases significantly. The response of the moderately ductile walls to amplified ground motion records was not investigated given that none of the employed ground motion records incurred in inelastic response of these walls.

Fig. 6 (a) and (b) illustrate the lateral response of Wall DSRW along with that of Wall DHW when subjected to Record 150 - Coyote Lake, 1979 amplified by 150% and 200%, respectively. The displaced shape of the walls at the end of the analyses using the amplified records is presented in Fig. 7, along with the cracking pattern. Although both walls experience comparable levels of peak roof displacement, Wall DHW is notably more effective in minimizing the permanent displacements at the end of the excitation, particularly under the 200% earthquake. The greater recovery capacity of the SMA-reinforced wall is evident when comparing the permanent displaced shapes of Wall DHW in Fig. 7 (b) and Fig. 7 (d) with the respective shape of Wall DSRW in Fig. 7 (a) and Fig. 7 (c).

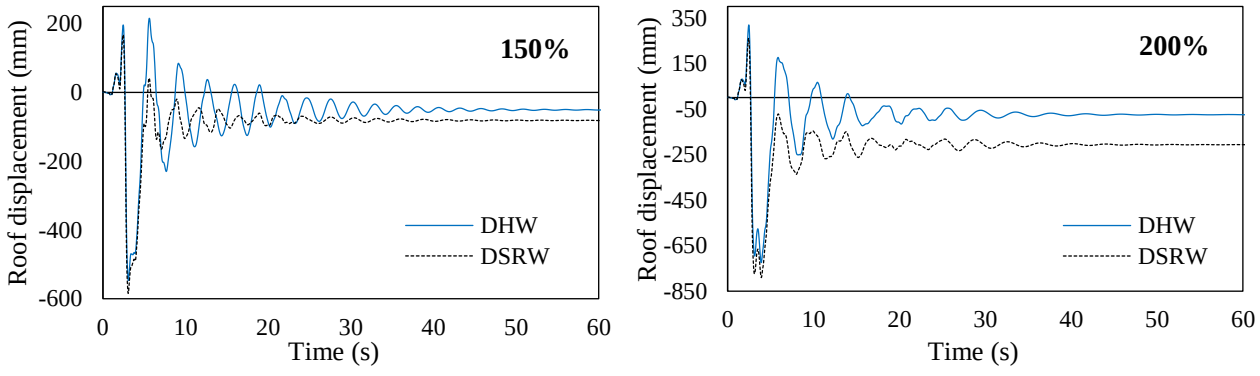

Fig. 6 – Roof displacement time histories of ductile walls under Record 150 amplified by: (a) 150% and (b) 200%

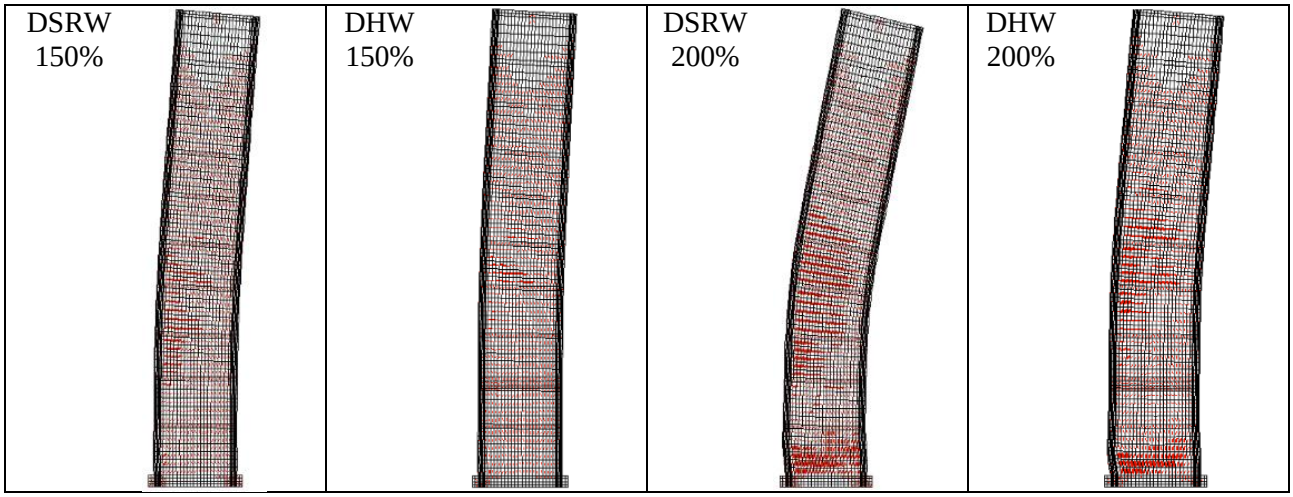

Fig. 7 – Permanent displaced shape of ductile walls under amplifications of Record 150

The peak and permanent roof displacements of the ductile walls under the amplified Record 150 are summarized in Table 5, while the peak and the permanent interstorey drifts are illustrated in Fig. 8 (a) and Fig. 8 (b), respectively. Wall DHW experienced smaller peak roof drifts compared to Wall DSRW in both analyses, corresponding to an average reduction of 25%. The roof drift sustained by Wall DHW at the end of analysis was 60% of that sustained by Wall DSRW at 150% excitation, and 36% of that relative to the 200% excitation. Wall DHW exhibited similar recovery capacity under the two levels of excitation. Wall DSRW exhibited lower recovery under the amplified record to 150%, which was further reduced under the amplification of 200%. Therefore, the recovery capacity of Wall DHW was 6.5% greater at 150% amplification, and 22% greater at 200% amplification, compared to Wall DSRW.

Table 5 – Roof displacements of ductile walls under Record 150 amplified

Amplification of Record 150	**150%**		**200%**	
Wall	**DSRW**	**DHW**	**DSRW**	**DHW**
Peak roof displacement mm (drift)	585 (1.9%)	547 (1.8%)	790 (2.6%)	724 (2.4%)
Permanent roof displacement mm (drift)	82 (0.3%)	49 (0.2%)	207 (0.7%)	74 (0.2%)
Recovery of roof drifts	86%	91%	74%	90%

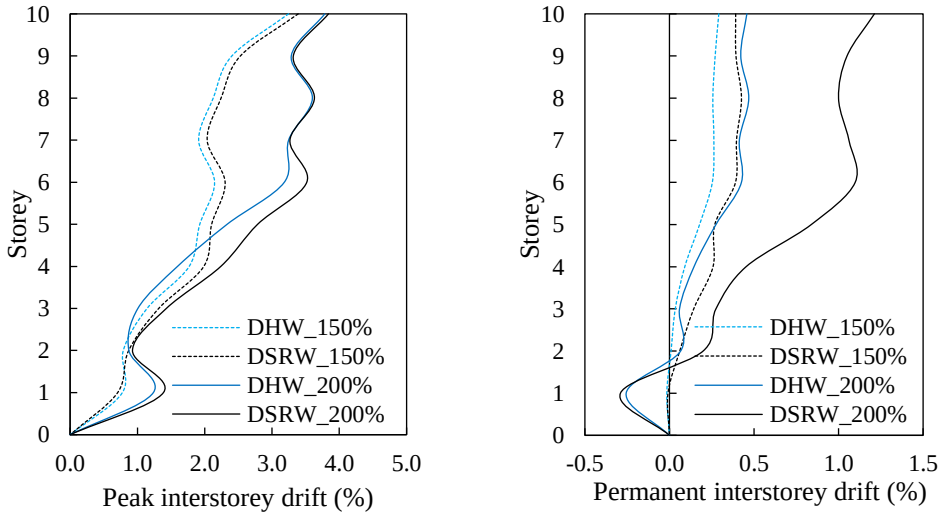

Fig. 8 – Interstorey drift response of ductile walls to amplified Record 150: (a) peak and (b) permanent

In terms of interstorey drifts, Wall DHW was able to recover most of the experienced interstorey drifts, particularly at storeys 5-7, where the longitudinal steel reinforcement yielded and substantial interstorey drifts were recorded, indicating the formation of a secondary plastic hinge in both walls. At storey 6, the interstorey drift in Wall DHW was 64% of that exhibited by Wall DSRW at 150% amplification, and 42% at 200% amplification. The SMA-reinforced wall performed better than the steel-reinforced wall in limiting the permanent drifts. The interstorey drifts along the height of the ductile walls also indicate that the SMA-reinforced wall was less susceptible to the negative effects of the secondary plastic hinge that formed at upper levels compared to the conventional steel-reinforced wall, which is further stressed by the improved performance of Wall DHW at 200% in terms of permanent interstorey drifts.

6. Conclusions

In this study, full-scale finite element models of ductile and moderately ductile shear walls were subjected to nonlinear time history analysis, in order to predict and compare the seismic performance of self-centering walls containing Ni-Ti superelastic SMA as alternative reinforcement in the plastic hinge region to that of conventional steel-reinforced walls. Simulated and historical ground motion records were selected and scaled to match the uniform hazard spectra of two design locations in Canada, corresponding to the high seismic zone of Vancouver and the moderate seismic zone of Montreal. Amplified ground motion records were also employed for the Vancouver location to capture the inelastic response of the walls to larger seismic demands.

In general, improved seismic performance was exhibited by the SMA-reinforced walls, specifically at higher seismic demands. The dynamic analyses demonstrated that self-centering of SMA-reinforced concrete shear walls reduces permanent drifts along the height of the walls. Furthermore, the SMA-reinforced walls experienced comparable transient peak drifts to the steel-reinforced walls despite their characteristic reduced stiffness and energy dissipation capacity.

For Vancouver, the SMA-reinforced wall DHW performed better than the steel-reinforced wall DSRW in limiting the permanent drifts by utilizing the recentering capability of superelastic Ni-Ti SMA, which was more evident under amplified ground motions. In addition, a secondary plastic hinge was observed at storeys 5-7 of the ductile walls DHW and DSRW. The SMA-reinforced wall was more effective in reducing the drifts at this location compared to Wall DSRW, resulting in an improved performance of the hybrid wall in terms of interstorey drifts.

For Montreal, few records induced displacements that were above the Δ_y of each wall, and by a negligible extent. Consequently, permanent damage exhibited by the walls was limited, and the response of the shear walls was not significantly improved by the presence of the SMA reinforcing bars. This indicates that the demand related to moderate seismic zones may not justify the use of self-centering SMA-reinforced concrete shear walls.

Less stringent limits on the fundamental period of the hybrid shear walls would potentially permit exploring the flexibility characteristic of SMA-reinforced concrete walls when determining the design base shear. In addition, the predicted fracture of the longitudinal steel reinforcement in the web zone of Wall DHW when subjected to the records from Scenario 3 indicates that the lateral capacity of the hybrid SMA-steel reinforced concrete walls was limited by the capacity of the steel bars. Therefore, appropriate seismic design provisions would potentially help designers to take full advantage of the improved performance of concrete walls containing SMA as reinforcement.

7. Acknowledgements

The first author gratefully acknowledges the financial support provided by York University, and by Mitacs through the Globalink Graduate Fellowship.

8. References

[1] Tarzav M, Saiidi MS (2015): Reinforcing NiTi Superelastic SMA for Concrete Structures. *Journal of Structural Engineering*, **141** (8), 0414197-1-10.

[2] Abraik E, Youssef MA (2015): Cyclic performance of shape memory alloy reinforced concrete walls. *Conference on Response of Structures under Extreme Loading*, East Lansing, USA.

[3] Abraik E, Youssef MA (2016): Performance assessment of three-story shape memory alloy reinforced concrete walls. *Resilient Infrastructure,* London, Canada, **852**, 1-9.

[4] Ghassemieh M, Rezapour M, Sadeghi V (2017): Effectiveness of the shape memory alloy reinforcement in concrete coupled shear walls. *Journal of Intelligent Material Systems and Structures*, **28** (5), 640-652.

[5] Abraik E, Youssef MA (2018): Seismic fragility assessment of superelastic shape memory alloy reinforced concrete shear walls. *Journal of Building Engineering*, **19**, 142-153.

[6] Kian MJT, Cruz-Noguez C (2018): Reinforced Concrete Shear Walls Detailed with Innovative Materials: Seismic Performance. *Journal of Composites for Construction*, **22** (6), 04018052-1-11.

[7] Cortés-Puentes WL, Zaidi M, Palermo D, Dragomirescu E (2018): Cyclic loading testing of repaired SMA and steel reinforced concrete shear walls. *Engineering Structures*, **168**, 128-141.

[8] Abdulridha A, Palermo D (2017): Behaviour and modelling of hybrid SMA-steel reinforced concrete slender shear wall. *Engineering Structures*, **147**, 77-89.

[9] Maciel M, Palermo D, Abdulridha A (2016): Seismic Response of SMA Reinforced Shear Walls. *Special Topics in Structural Dynamics*, vol. 6, chapter 9, 185-192, Bethel, USA.

[10] Maciel M (2019): Seismic performance analysis of mid-rise concrete shear walls reinforced with superelastic shape memory alloys. *MASc Thesis.* York University, Toronto, Canada.

[11] Sadeghian A (2018): Seismic deformations of taller Reinforced Concrete shear walls located in eastern Canada. *PhD Thesis*, University of Montreal, Montreal, Canada.

[12] CSA (2014): CSA-A23.3: Design of Concrete Structures. *Canadian Standard Association*, Mississauga, Canada.

[13] NRC (2015): Division B, Part4, Structural Design National Building Code of Canada. *National Research Council of Canada*, Ottawa, Canada.

[14] Cortés-Puentes WL, Palermo D (2017): SMA tension brace for retrofitting concrete shear walls. *Engineering Structures*, **140**, 177-188.

[15] Cortés-Puentes WL, Palermo D (2018): Modeling of Concrete Shear Walls Retrofitted with SMA Tension Braces. *Journal of Earthquake Engineering*, DOI: 10.1080/13632469.2018.1452804.

[16] Vecchio FJ, Wong P, Trommels H (2013): VecTor2 and Formworks Manual. *University of Toronto*, 2nd edition.

[17] Abdulridha A, Palermo D, Foo S, Vecchio FJ (2013): Behavior and modeling of superelastic shape memory alloy reinforced concrete beams. *Engineering Structures*, **49**, 893-904.

[18] Atkinson GM (2009): Earthquake time histories compatible with the 2005 National building code of Canada uniform hazard spectrum. *Canadian Journal of Civil Engineering*, **36**, 991-1000.

[19] Tremblay R, Atkinson GM, Bouaanani N, Daneshvar P, Léger P, Koboevic S (2015): Selection and scaling of ground motion time histories for seismic analysis using NBCC 2015. *The 11th Canadian Conference on Earthquake Engineering*, Victoria, Canada.

[20] Ancheta TD, Darragh RB, Stewart JP, Seyhan E, Silva WJ, Chiou BSJ, Wooddell KE, Graves RW, Kottke AR, Boore DM, Kishida T, Donahue JL (2013): PEER NGA-West2 Database. *PEER Report 2013/03*, Pacific Earthquake Engineering Research, Berkeley, USA.

[21] Alam MS, Nehdi M, Youssef MA (2009): Seismic Performance of Concrete Frame Structures Reinforced with Superelastic Shape Memory Alloys. *Smart Structures and Systems*, **5** (5), 565-585.

